Wang, L., Hainzl, S., Sinan Özeren, M., Ben-Zion, Y. (2010): Postseismic deformation induced by brittle rock damage of aftershocks. - Journal of Geophysical Research, 115, B10422

DOI: 10.1029/2010JB007532

Postseismic deformation induced by brittle rock damage of aftershocks

Lifeng Wang,[1,2] Sebastian Hainzl,[1] M. Sinan Özeren,[3] and Yehuda Ben-Zion[4]

Received 8 March 2010; revised 18 June 2010; accepted 2 July 2010; published 30 October 2010.

[1] Large earthquakes are commonly followed by abundant aftershocks that are densely located around the coseismic rupture zone. Laboratory experiments indicate that "microscopic" brittle rock failures (acoustic emission) are associated collectively with a "macroscopic" damage-related inelastic relaxation. Utilizing basic relations between local brittle failures and gradual inelastic strain in a viscoelastic damage rheology model, we develop connections between aftershock decay rates and the aftershocks-induced component of geodetic deformation. The discussed mechanism is relevant for postseismic relaxation produced by sources located within the seismogenic zone, and especially in regions that overlap locations of high aftershocks activity. Assuming the Omori-Utsu decay rate for aftershocks, we find that the temporal decay of the damage-related postseismic relaxation follows a generalized power-law relation with the standard Omori-Utsu law as a limit case. The results provide a way for estimating the separate contributions to observed postseismic displacements that stem from brittle failures in the seismogenic zone (aftershocks) and other (aseismic) processes. Using the obtained theoretical expectations, we analyze postseismic displacements measured by GPS stations around the North Anatolian fault ~3 months following the 1999 M7.4 İzmit earthquake. We find that the observed postseismic displacements decay slower than the aftershock seismicity. Based on our theoretical results, we conclude that up to 50% of the measured surface displacements at near-fault sites can be attributed to aftershock-induced inelastic deformation in the seismogenic zone. The remainder postseismic deformation can generally be explained by relaxation in the deeper ductile substrate.

Citation: Wang, L., S. Hainzl, M. Sinan Özeren, and Y. Ben-Zion (2010), Postseismic deformation induced by brittle rock damage of aftershocks, *J. Geophys. Res.*, *115*, B10422, doi:10.1029/2010JB007532.

1. Introduction

[2] Postseismic deformation following the occurrence of large earthquakes has long been detected by means of geodetic measurements [e.g., *Shen et al.*, 1994; *Savage and Svarc*, 1997; *Bürgmann et al.*, 1997; *Ergintav et al.*, 2002; *Ryder et al.*, 2007]. Several physical models have been proposed to explain the postseismic relaxation processes. The commonly assumed mechanisms are (1) poroelastic effects associated with fluid motion in saturated rocks [e.g., *Nur and Byerlee*, 1971; *Rice and Cleary*, 1976; *Wang*, 2000], (2) stable aseismic motion on highly localized surfaces above and below the seismogenic zone referred to as afterslip [e.g., *Marone et al.*, 1991], and (3) viscoelastic relaxation in distributed horizontal asthenospheric layer or in localized deep ductile shear zone [e.g., *Thatcher*, 1983; *Li and Rice*, 1987; *Ben-Zion et al.*, 1993; *Montési*, 2004]. In this study we develop quantitative results associated with a fourth category of postseismic deformation involving directly the inelastic relaxation produced by the occurrence of multitudinous aftershock events. To provide a context for our results, we discuss below general aspects of the commonly assumed mechanisms and observations.

[3] Poroelastic rebound occurs when fluid in saturated rocks diffuse in response to coseismic stress perturbations. The fluid diffusion and associated pore pressure changes produce transient strain field in the crust. It has been reported that poroelastic rebound following large earthquakes occurs at shallow depths and significantly at step-over regions of fault zones [e.g., *Peltzer et al.*, 1998; *Masterlark and Wang*, 2002]. The time dependency of this relaxation process is complicated, and usually the difference between displacement fields of two end-member models (undrained and drained) is calculated to analyze the fluid effects [e.g., *Fialko*, 2004; *Jónsson et al.*, 2003]. In comparison, the afterslip process is assumed to be associated with rate-strengthening friction on extensions of the seismogenic (rate-weakening) portion of the fault [e.g., *Scholz*, 1998; *Marone and Scholz*,

[1]Deutsches GeoForschungsZentrum, Potsdam, Germany.
[2]China Earthquake Networks Center, China Earthquake Administration, Beijing, China.
[3]Istanbul Technical University, Istanbul, Turkey.
[4]Department of Earth Sciences, University of Southern California, Los Angeles, California, USA.

0148-0227/10/2010JB007532

1988; *Blanpied et al.*, 1991; *Chester*, 1995]. This process is expected to produce postseismic deformation with logarithmic time-dependency [*Marone et al.*, 1991] and has been used in several recent analyses of observed data [e.g., *Hearn et al.*, 2009; *Perfettini and Avouac*, 2004; *Savage and Svarc*, 2009]. The viscoelastic relaxation process is assumed to be dominant in the deeper and hotter asthenosphere below the seismogenic zone. This has been modeled by linear rheology with various combinations of Maxwell and Kelvin elements [e.g., *Pollitz et al.*, 2000], power-law rheology [e.g., *Freed and Bürgmann*, 2004], and localized nonlinear viscous flow in a ductile shear zone [*Montési*, 2004]. Viscoelastic relaxation governed by linear viscosity has either exponential or logarithmic temporal decay depending on the employed rheological elements considered [*Hetland and Hager*, 2006], while a localized nonlinear viscous flow has power-law decay with time [*Montési*, 2004].

[4] The differences in the nature of the above three deformation mechanisms lead to some differences in the displacement fields at the surface. For strike-slip events, which are the focus of this work, poroelastic rebound produces displacements generally opposite to those generated by the mainshocks, as indicated, e.g., following the 1992 Landers earthquake [*Peltzer et al.*, 1998; *Fialko*, 2004] and two 2000 M_w6.5 earthquakes in Iceland [*Jónsson et al.*, 2003]. On the other hand, both afterslip and viscoelastic relaxation produce similar kinematic motions as the mainshocks. It is thus comparatively easy to recognize poroelastic rebound, but still a challenge to distinguish between afterslip and viscous flow based on displacement or velocity measurements [e.g., *Thatcher*, 1983]. The displacement time series may provide more information for distinguishing among the latter two mechanisms [*Wang et al.*, 2009].

[5] Some further constraints on the relevant physical mechanisms may be provided by the inferred locations of the operating sources. Several studies found that the postseismic relaxation following various earthquakes is principally on the fault continuation beneath the coseismic rupture and can be attributed to frictional-afterslip (perhaps combined with localized viscoelastic relaxation). Examples include the 1999 *M*7.1 Hector Mine [*Owen et al.*, 2002] and the 2003 *M*6.5 Chengkung [*Hsu et al.*, 2009] events. On the other hand, many studies have shown that some early postseismic relaxation following large events is associated with sources located *within* the seismogenic zone (as well as at very shallow depth). Examples include the 1989 Loma Prieta [*Pollitz et al.*, 1998], 1999 *M*7.4 İzmit [*Bürgmann et al.*, 2002; *Wang et al.*, 2009], and the 2003 *M*6.9 Boumerdes (Algeria) [*Mahsas et al.*, 2008] earthquakes. The frequently observed postseismic deformation within the seismogenic zone does not have an obvious explanation using strictly either deep viscous flow or aseismic frictional-afterslip. In particular, many inferred locations of significant postseismic deformation appear to be in areas of high seismic activity (see more details below), where rate-weakening friction associated with brittle instabilities is expected. It is thus possible that an additional mechanism of postseismic relaxation, associated closely with brittle instabilities, is operating within the seismogenic zone.

[6] In addition to the observed geodetic deformation, aftershocks are significant markers of the relaxation processes following large earthquakes. Some similarities have been found between aftershocks and geodetic deformation. First, both have generally consistent kinematic motion with the mainshocks [*Bürgmann et al.*, 2002; *Hsu et al.*, 2002; *Bohnhoff et al.*, 2006]. Second, an Omori-type decay which is well-known for aftershock sequences has also been noticed for the postseismic displacements recorded by continuous GPS measurements following, e.g., the 1999 Chi-Chi earthquake [*Perfettini and Avouac*, 2004; *Savage et al.*, 2007] and 2001 *M*8.4 Peru earthquake [*Perfettini et al.*, 2005]. Some investigations also indicated spatial correlations between aftershocks and postseismic relaxation sources inferred from slip inversion. For example, *Miyazaki et al.* [2004] showed that the aftershocks of the 2003 Tokachi-oki earthquake overlap the postseismic slip area inferred from the GPS measurements. Similar spatial correlations have also been found following, e.g., the Chi-Chi earthquake [*Yu et al.*, 2003] and 2005 *M*8.7 Nias-Simeulue event [*Hsu et al.*, 2006]. It was also reported that most of the postseismic deformation following the 2003 *M*7.3 Altai earthquake can be explained by seismic moment release in aftershocks [*Barbot et al.*, 2008].

[7] Aftershocks are mainly located within the seismogenic volume affected by the mainshock-induced stress field and brittle deformation processes. Geological and geophysical studies indicate that large faults are surrounded by tabular damage zones with reduced elastic moduli compared to the host rocks [e.g., *Chester et al.*, 1993; *Ben-Zion et al.*, 2003; *Fialko et al.*, 2002]. In addition, recent seismological studies documented clear temporal changes in the elastic properties of fault damage zones following the occurrence of large earthquakes [e.g., *Sawazaki et al.*, 2006; *Peng and Ben-Zion*, 2006; *Rubinstein et al.*, 2007; *Wu et al.*, 2009]. It is reasonable to assume that similar changes of elastic moduli accompany locally the occurrence of aftershocks, especially in space-time domains with high seismicity rates.

[8] *Ben-Zion and Lyakhovsky* [2006] analyzed aftershocks in a viscoelastic damage rheology model, based on nonlinear continuum mechanics and thermodynamics, for evolving elastic properties and related deformation patterns in rocks sustaining irreversible brittle deformation. The effective elastic moduli in the damage model are functions of an evolving nondimensional state variable $0 \leq \alpha \leq 1$ representing the local crack density [*Lyakhovsky et al.*, 1997]. The evolution of the microcrack density during local brittle failures (e.g., aftershocks) changes the effective viscosity of the medium and leads to gradual overall inelastic deformation [*Hamiel et al.*, 2004].

[9] In the present paper we derive quantitative connections between the expected postseismic deformation and changes of the effective viscosity of the crust generated collectively by aftershock sequences. Following basic relations of the damage rheology model [*Ben-Zion and Lyakhovsky*, 2006], we quantify the aftershocks-induced component of the postseismic geodetic deformation. The obtained results provide a useful tool for separating the aftershocks/damage-related postseismic deformation from the commonly assumed aseismic deformation mechanisms (e.g., afterslip or viscoelastic relaxation). Assuming that the decay rate of aftershocks obeys the Omori-Utsu law, we show in section 2 that the time evolution of the damage-related postseismic deformation follows a generalized Omori-type decay, with the standard Omori-Utsu law as a limit case. In section 3 we apply the derived expressions to the postseismic deforma-

tion field recorded following the 1999 Izmit earthquake in Turkey. The results are discussed in section 4 and summarized in section 5.

2. Time Evolution of Aftershocks-Induced Aseismic Deformation

2.1. Deformation in a Viscoelastic Damage Model

[10] Detailed reviews of the damage model in relation to aftershocks can be found in articles by *Ben-Zion and Lyakhovsky* [2006] and *Ben-Zion* [2008]. Below we summarize the main ingredients of the model that are relevant for the present work. The total deformation field in the viscoelastic damage model can be written, in analogy with Maxwell viscoelasticity, as the sum of three strain components:

$$\varepsilon_{ij}^{t} = \varepsilon_{ij}^{e} + \varepsilon_{ij}^{i} + \varepsilon_{ij}^{d}, \tag{1a}$$

where ε_{ij}^{e} is elastic strain, ε_{ij}^{i} denotes a damage-related inelastic strain, and ε_{ij}^{d} represents a (nonbrittle) ductile strain. In a simple model consisting of a brittle seismogenic zone over a ductile substrate, the third term in equation (1a) may be assumed to be zero in the seismogenic zone, while the first two terms may be neglected in the ductile substrate. For a simplified situation of uniform deformation in a single direction, equation (1a) may be replaced by the corresponding scalar version:

$$\varepsilon^{t} = \varepsilon^{e} + \varepsilon^{i} + \varepsilon^{d}. \tag{1b}$$

[11] For a 1-D case of uniform deformation, the relation between the stress σ and elastic strain in the damage model is given [*Ben-Zion and Lyakhovsky*, 2006] by

$$\sigma = 2\mu_0(1-\alpha)\varepsilon^{e}, \tag{2a}$$

where μ_0 is the initial rigidity of the undamaged solid, $0 \leq \alpha \leq 1$ is the damage state variable and $\mu_0(1-\alpha)$ is the effective elastic modulus of the damaged solid.

[12] Analysis of stress-strain and acoustic emission data of fracturing experiments [*Hamiel et al.*, 2004] indicates that the inelastic strain rate in a gradual distributed damage process (e.g., aftershocks), not associated with large localized system-size instabilities (e.g., mainshocks), can be described by

$$\dot{\varepsilon}^{i} = C_v\dot{\alpha}\sigma, \tag{2b}$$

where C_v is a material constant and the product $C_v\dot{\alpha}$ represents the inverse of an effective damage-related viscosity that decreases with increasing damage rate (e.g., aftershocks rate). When the damage rate approaches zero, the effective viscosity becomes infinite, and the system enters a phase of interseismic deformation associated with purely elastic behavior and healing (recovery) of the effective elastic properties (this behavior is not analyzed here). Equation (2b) provides a constitutive relation only for the period associated with the occurrence of ongoing distributed brittle instabilities leading to material degradation. A more complete description that includes also the longer interseismic period, when the healing process leads to material recovery, can be found in articles by *Lyakhovsky et al.* [1997, 2001].

[13] Over relatively short time intervals after the occurrence of mainshocks, the total strain in a volume around the fault can be assumed to be approximately constant [*Ben-Zion and Lyakhovsky*, 2006; *Ben-Zion*, 2008] and unaffected by changes in the ductile substrate. In this case, the rate of elastic strain relaxation in the seismogenic zone is equal to the rate of increasing inelastic strain in the volume containing the aftershocks. From equation (1b) with zero ductile component in the seismogenic zone, this can be written as $2\dot{\varepsilon}^{e} = -\dot{\varepsilon}^{i}$, where the factor 2 stems from the common definitions of the strain and strain-rate tensors and the overdots denote time derivatives [*Ben-Zion and Lyakhovsky*, 2006].

2.2. Omori-Type Decay for Damage-Related Postseismic Deformation

[14] Combing equations (2a) and (2b) yields

$$\dot{\varepsilon}^{i} = 2R\dot{\alpha}(1-\alpha)\varepsilon^{e}, \tag{3}$$

with $R = \mu_0 C_v$. As shown by *Ben-Zion and Lyakhovsky* [2006], the nondimensional material parameter R characterizes the ratio of the timescales of brittle damage generation over Maxwell viscous relaxation and is also inversely proportional to the degree of seismic coupling in a region. Applying the constant strain boundary condition, as described above, the elastic strain rate is

$$\dot{\varepsilon}^{e} = -R\dot{\alpha}(1-\alpha)\varepsilon^{e}. \tag{4}$$

Integration of equation (4) provides elastic strain in the form

$$\varepsilon^{e} = \varepsilon_0 A e^{\frac{1}{2}R(1-\alpha)^2}, \tag{5}$$

where $A = e^{-\frac{1}{2}R(1-\alpha_0)^2}$ with α_0 and ε_0 being the damage state and elastic strain at $t = 0$. Replacing ε^{e} in equation (3) by equation (5), the inelastic strain rate is

$$\dot{\varepsilon}^{i} = 2R\varepsilon_0 A(1-\alpha)\dot{\alpha}e^{\frac{1}{2}R(1-\alpha)^2}. \tag{6}$$

[15] The damage state variable (α), which represents the local microcrack density in a rock volume, should be correlated with the aftershock activity during the postseismic time interval. The generated brittle damage is expected to be proportional to the total rupture area of the events. Since the generated brittle damage is expected to be proportional to rupture area A of the events, we assume a linear relationship between α and the cumulative rupture area,

$$\alpha = \alpha_0 + \varphi' \sum_{i=1}^{N} A_i \tag{7a}$$

where N is the number of aftershocks, α_0 denotes the initial damage, and φ' is a constant. This can be simplified to

$$\alpha = \alpha_0 + \varphi N \tag{7b}$$

where $\varphi = \varphi'\langle A_i\rangle$ with $\langle A_i\rangle$ being the average rupture area of the events above some magnitude threshold. Equation (7b) is consistent with the relation used by *Ben-Zion and Lyakhovsky* [2006] and is used below. Replacing α in

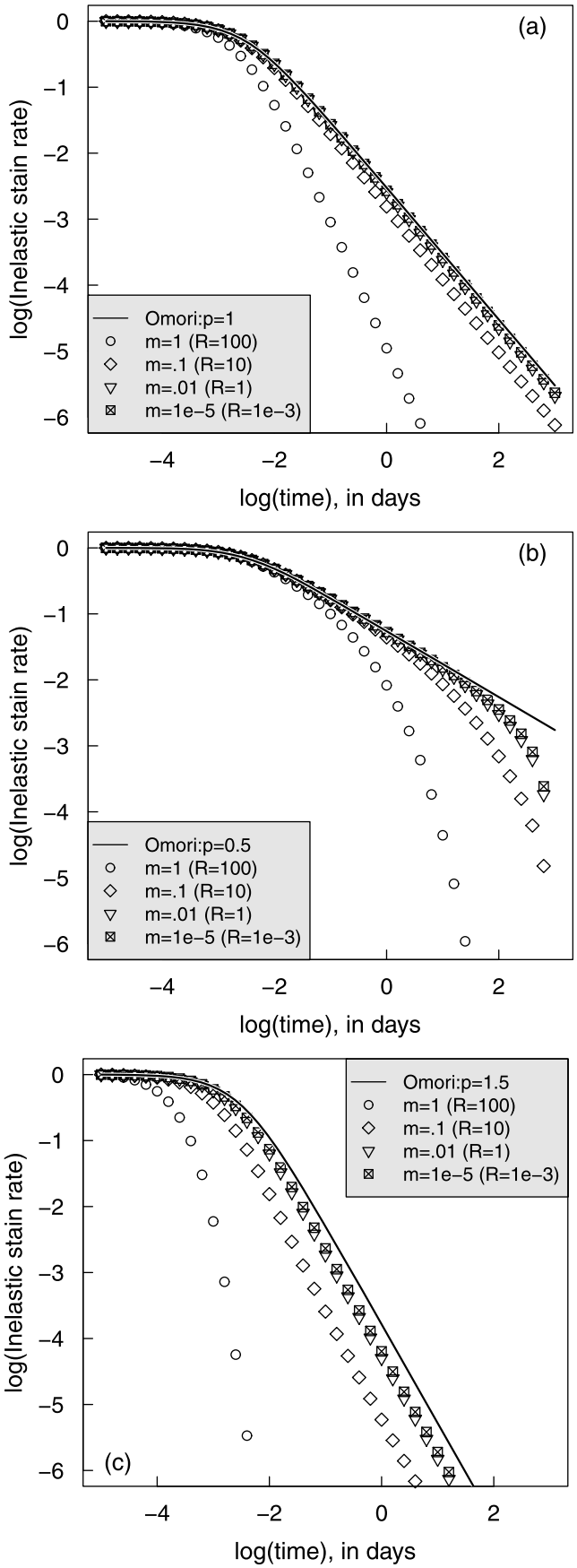

Figure 1. Normalized inelastic strain rate as a function of time based on equation (8) for (a) $p = 1$, (b) $p = 0.5$, and (c) $p = 1.5$. We assume $\alpha_0 = 0.25$, $\varphi = 10^{-4}$, $K = 133$, and $c = 0.003$ days. The inelastic strain rate with different m (or R) parameters is shown by different labels. The solid curves show results (labeled as 'Omori') based on the Omori-Utsu law.

equation (6) with equation (7b), we get the damage-related inelastic strain stemming from aftershock seismicity as

$$\dot{\varepsilon}^i = 2R\varepsilon_0(1-\alpha_0-\varphi N)\varphi\dot{N}e^{-(1-\alpha_0)R\varphi N+\frac{1}{2}R(\varphi N)^2}. \quad (8)$$

[16] The time-dependency of inelastic strain in equation 8 can be obtained by applying the classical Omori-Utsu law for the aftershock occurrence rate [*Utsu et al.*, 1995],

$$\dot{N}(t) = \frac{K}{(c+t)^p}, \quad (9)$$

where K, c, and p are constants. The total number of aftershocks is $N(t) = K \cdot g(t)$ with

$$g(t) = \begin{cases} \ln(1+t/c), & p = 1 \\ \dfrac{(c+t)^{1-p} - c^{1-p}}{1-p}, & p \neq 1 \end{cases}. \quad (10)$$

[17] When $\varphi N \ll 1 - \alpha_0 < 1$, which is appropriate for the short time period of months following a large earthquake, we can neglect the quadratic term $(\varphi N)^2$ in the exponential term and only consider the linear dependence on φN,

$$\dot{\varepsilon}^i \cong 2R\varepsilon_0(1-\alpha_0-\varphi N)\varphi\dot{N}e^{-(1-\alpha_0)R\varphi N}. \quad (11)$$

Defining

$$m = R(1-\alpha_0)\varphi K, \quad (12)$$

we have for $p = 1$,

$$\dot{\varepsilon}^i = 2m\varepsilon_0 c^m[1-\beta\cdot g(t)]\frac{1}{(c+t)^{1+m}} \quad (13)$$

and

$$\varepsilon^i = 2\varepsilon_0\left[1-\frac{\beta}{m}\right] - 2\varepsilon_0\left[1-\frac{\beta}{m}-\beta\cdot g(t)\right]\left(1+\frac{t}{c}\right)^{-m}, \quad (14)$$

with $\beta = \frac{\varphi K}{1-\alpha_0} \ll 1$. Equation 14 gives as expected $\varepsilon^i = 0$ for $t = 0$. We note that when β is a small value, the time evolution of inelastic strain rate in equation 13 is dominated by the last term $(\frac{1}{(c+t)^{1+m}})$, which provides a generalized Omori-type decay.

[18] Figure 1 displays the normalized inelastic strain rate described by equation 8 (without approximation) for different m (or R) values, assuming constants $\alpha_0 = 0.25$, $\varphi = 10^{-4}$ [*Ben-Zion and Lyakhovsky*, 2006], $K = 133$, and $c = 0.003$ days [*Enescu et al.*, 2007]. The three plots correspond to the cases of $p = 1$, 0.5 and 1.5, respectively. As seen, the m (or R) parameter determines the decay behavior of the inelastic strain. Small m (or R) values produce a slow decay of inelastic strain, while large m (or R) values indicate a fast decay behavior. This is consistent with the 3-D simulations of aftershock sequences in the work of *Ben-Zion and*

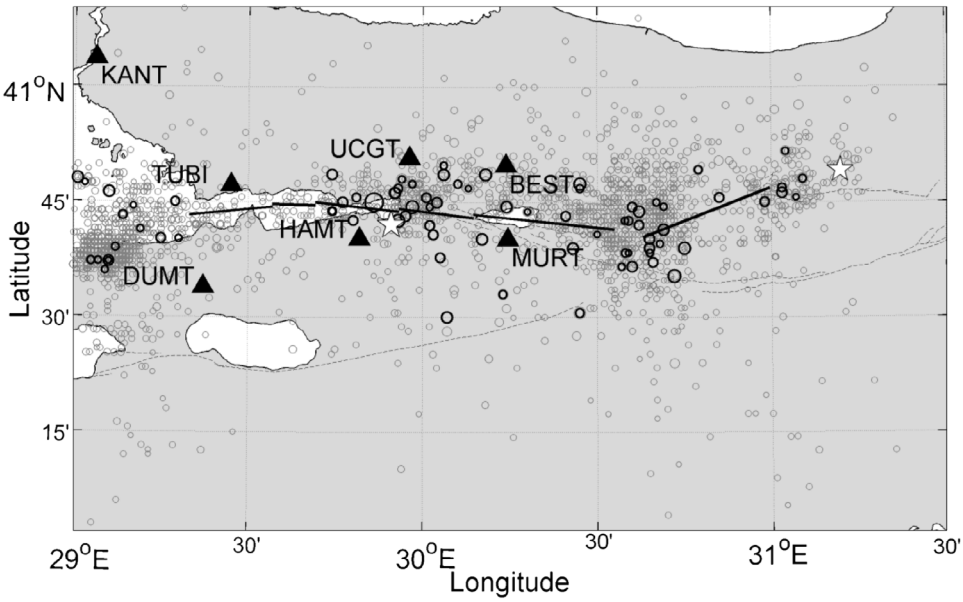

Figure 2. Locations of the GPS stations (black triangles) and the spatial distribution of observed aftershocks (gray circles, $M \geq 2.5$) in the first 87 days following the İzmit earthquake. Aftershocks with magnitude larger than 4.0 are highlighted by black circles. White stars display the epicenters of the İzmit (40.76°N, 29.97°E) and Düzce (40.82°N, 31.20°E) earthquakes. Black solid lines show the rupture trace of the İzmit earthquake [*Wright et al.*, 2001]. The gray dotted lines mark a simplified location of the North Anatolian fault [*Lorenzo-Martín et al.*, 2006]. The aftershocks catalog is from the Kandilli Observatory and the Earthquake Research Institute (Istanbul, Turkey).

Lyakhovsky [2006]. They demonstrated that small (vs. large) R values, associated with a more brittle (vs. viscous) rheology, produce long (vs. short) aftershock sequences with slow (vs. fast) decay. Figure 1 also indicates that the damage-related inelastic strain should decay faster than the seismicity. If we denote with p_d and p_s the exponents in the Omori-Utsu law for the damage-related inelastic strain and the aftershocks, respectively, the forgoing results imply that $p_d > p_s$. This conclusion can also be drawn directly from equation 13 for the special case of $p = 1$.

[19] If the inelastic strain rate obeys equation 8, the damage-related postseismic deformation $D(t)$ that is proportional to inelastic strain (i.e., $D(t) \sim \varepsilon^i$ [*Montési*, 2004]) is determined by equation 8 as well. The scaling parameter between the damage-related postseismic deformation and inelastic strain can be lumped into the proportionality factor of equation 8. In the following sections we investigate the decay behaviors of the aftershocks and postseismic displacement following the 1999 İzmit earthquake. The derived results are used first to analyze the contribution of aftershocks-induced postseismic deformation, and then to estimate the relative contributions of the brittle and nonbrittle components of deformation in the observed postseismic GPS data at different locations.

3. Analysis of Observed Postseismic Displacements Following the İzmit Earthquake

3.1. Summary of Key Observations and Previous Analyses

[20] The 17 August 1999 M7.4 İzmit earthquake (40.76°N, 29.97°E) was a devastating event that occurred on the North Anatolian Fault Zone (NAFZ) and caused many casualties. It was followed by the 12 November 1999 M7.2 Düzce earthquake after 87 days. The İzmit earthquake ruptured over 150 km long section of the NAFZ, from the Sea of Marmara in the west to Düzce in the east. Because the Marmara Sea region was identified as a seismic gap likely to generate large earthquakes [*Toksöz et al.*, 1979], GPS monitoring was active before the 1999 event and was intensified after the İzmit mainshock to track early postseismic deformation. This allowed capturing the early time-varying postseismic displacement field by geodetic measurements. The locations of the GPS stations and aftershock epicenters in the study region are shown in Figure 2.

[21] Several studies inverted the post İzmit GPS data [*Bürgmann et al.*, 2002; *Çakir et al.*, 2003; *Wang et al.*, 2009; *Ergintav et al.*, 2009] and interferometric synthetic aperture radar (InSAR) measurements [*Çakir et al.*, 2003] for stable slip on the extended coseismic fault plane. Except for some details in the inverted patterns, these studies generally show similar slip concentrations. The results commonly indicate that the postseismic relaxation was focused primarily at relatively shallow depth (in the seismogenic zone) in the first days to 1–3 months. *Çakir et al.* [2003] also showed that the inferred postseismic deformation in the first month was overlapping or near the high seismic area according to the relocated aftershock catalog.

[22] The observed postseismic GPS displacements have been modeled assuming nonlinear viscous flow in the deep ductile shear zone [*Montési*, 2004] and distributed viscoelastic relaxation in the mantle [*Hetland*, 2006; *Hearn et al.*, 2006]. *Hearn et al.* [2002, 2009] modeled the postseismic displacements in the first several months based on frictional-

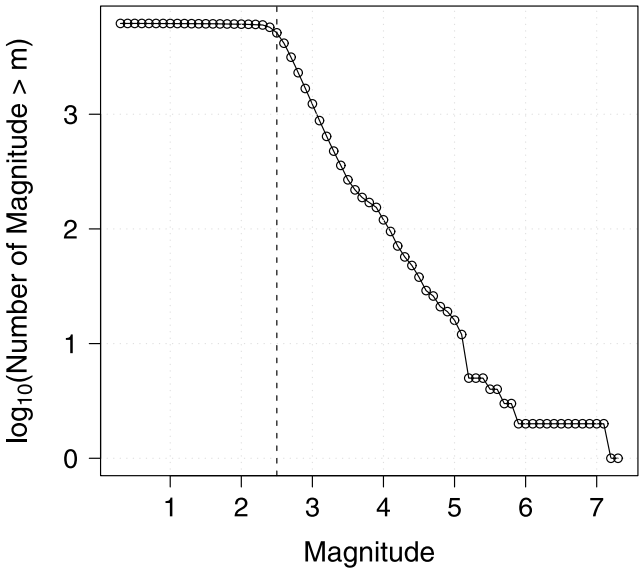

Figure 3. Frequency-magnitude statistics of the employed aftershocks. The catalog, from the Kandilli Observatory and Earthquake Research Institute, has a 1-day gap between 20 and 21 August 1999. The gap is filled up using the catalog managed by the ESRI of the Marmara Research Center, TÜBİTAK.

afterslip, assuming rate-strengthening friction along the extended coseismic fault plane above 2 km and below 10 km depth. Their obtained afterslip model indicates more significant creep at the shallow depth than at the deep section, implying a strong early postseismic relaxation near the surface. In addition, they found that the fictional-afterslip model is not able to produce sufficient postseismic deformation in the vicinity of the İzmit rupture and can only explain 63% of the observed early postseismic displacements. Generally speaking, neither frictional-afterslip [*Hearn et al.*, 2002, 2009] nor viscoelastic relaxation [*Montési*, 2004; *Hetland*, 2006] can fully explain the observed early shallow postseismic relaxation, especially in places overlapping concentrations of aftershocks. It has also been reported that poroelastic rebound is not able to fit the early postseismic displacements [*Hearn et al.*, 2002]. Thus, it is likely that a large portion of the early İzmit postseismic displacements is related to the aftershocks in the fault zone and may be induced by damage-related inelastic deformation.

[23] *Ergintav et al.* [2009] found that three logarithmic terms with characteristic decay times of 1, 150, and 3,500 days are necessary to fit the displacement time series over 7 years following the İzmit event. The term with a decay time of 1 day is characterized by strong fault-parallel motion originated from the seismogenic zone. The other two terms with longer decay constants describe either localized deep afterslip or viscoelastic relaxation and produce more broadly distributed strain with a symmetric double-couple pattern. Their detected early relaxation phase with short decay time of 1 day might be related to the aftershocks-induced inelastic deformation.

[24] In the following we apply our model to the postseismic displacements observed after the İzmit earthquake and investigate the relative contributions of the damage-related component and the aseismic components of the observed geodetic field at different locations. We first model the time evolution of the observed aftershock rates and postseismic geodetic deformation in order to compare their decay behaviors. Using the theoretical results of section 2, we then try to separate the three deformation components described in equation 1, which contribute to the postseismic displacement observed at the surface.

3.2. Omori-Utsu Decay of the Aftershocks

[25] We mainly use the aftershock catalog from the Kandilli Observatory and Earthquake Research Institute (Istanbul, Turkey). The magnitudes of the events were selected keeping, by order of availability, M_w, M_L, M_S, *mb*, and M_D [*Daniel et al.*, 2006]. The catalog probably misses numerous aftershocks in the first days after the mainshock, leading to inaccurate estimate of the onset time of the power law decay in the Omori-Utsu law [e.g., *Lolli and Gasperini*, 2006]. This catalog also has a 1 day gap between 20 August (day 3 from the İzmit earthquake) and 21 August 1999. We fill the gap using the catalog managed by the Earth Sciences Research Institute (ESRI) of the Marmara Research Center, TÜBİTAK. ESRI deployed a very dense network of seismic stations for monitoring the aftershock activity following the İzmit earthquake [*Aktar et al.*, 2004]. Based on the validity of the Gutenberg-Richter statistics for the observed moderate events (Figure 3), we consider the catalog complete for earthquakes with magnitude above $M_c = 2.5$.

[26] The aftershocks of the İzmit earthquake extended over an area of 40 by 170 km (Figure 2). Our investigations focus on the fault zone (approximately less than 10 km distance perpendicular to the fault according to the aftershock distribution), where the aftershocks densely occurred. We analyze the time period of the first 87 days after the İzmit mainshock, which is before the Düzce earthquake, using the modified Omori-Utsu law (Figure 4). The obtained parameters of the Omori-Utsu relation for the aftershocks ($M \geq 2.5$) around the rupture zone are $K_s = 86.95 \pm 0.39$, $c_s = 0.74 \pm 0.07$ days, and $p_s = 0.87 \pm 0.05$. As noted in section 2, the subscript *s* is used to distinguish the parameter estimates based on the seismicity from those derived in the next section based on the postseismic displacements. Because of the incompleteness of the catalog immediately after the large mainshock, the estimated c_s value might be inaccurate and larger than the true value [e.g., *Peng et al.*, 2006; *Enescu et al.*, 2007].

3.3. Time-Dependent Postseismic Deformation

[27] We use continuous GPS measurements recorded at seven stations located mostly near the fault (black triangles in Figure 2). Two GPS stations (TUBI, DUMT), which belong to MAGNET network, were operating before the İzmit earthquake. Four additional continuously recording GPS stations were installed in the 2 days following the mainshock. Stations UCGT and BEST are located less than 15 km north of the fault, and stations HAMT and MURT are approximately 5 km south of the İzmit rupture. In addition to the six stations near the fault, continuous GPS data at station KANT ~35 km from the fault is also included in the study.

[28] The İzmit earthquake is a continental strike-slip event with dominant postseismic motion in horizontal directions. Instead of treating the E-W and N-S GPS measurements

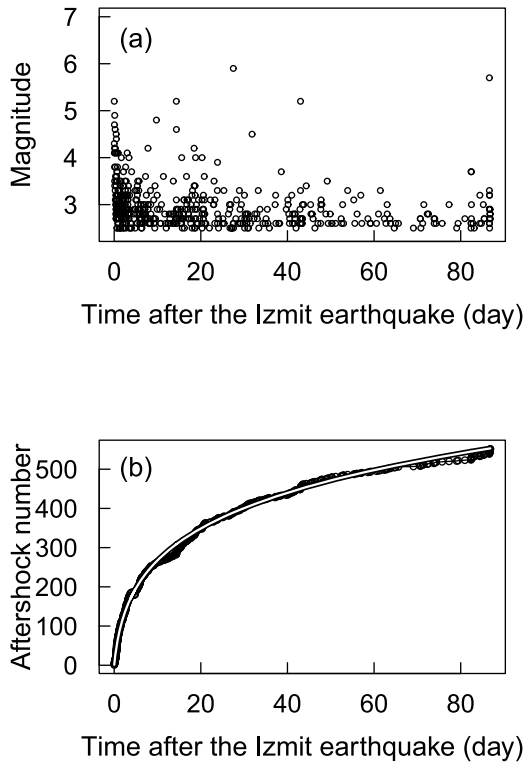

Figure 4. (a) Aftershocks ($M \geq 2.5$) around the rupture zone (less than 10 km distance perpendicular to the fault) versus time, and (b) the modeling result (white curve) using the Omori-Utsu power law relation.

separately, we utilize the principal component of the motion defined as $D = \sqrt{D_E^2 + D_N^2}$ with an azimuth of $\beta = atg(D_E/D_N)$. It has been shown that the azimuth of the principal displacement is relatively stable in the short time period of months following the İzmit earthquake, but it can be different from site to site [*Bürgmann et al.*, 2002]. The corresponding measurement uncertainty is calculated by $\sqrt{sd_E^2 + sd_N^2}$, where *sd* denotes the standard deviation of a given component. The postseismic deformations are given by $D_E = D'_E + D_{E0}$ and $D_N = D'_N + D_{N0}$, where D'_E and D'_N represent the recorded displacement measurements starting from some days after the mainshock, and D_{E0} and D_{N0} represent the postseismic displacements that occurred immediately after the mainshock and have not been captured by the GPS measurements (e.g., HAMT station started to run from about 1 day after the İzmit mainshock). With these definitions the principal displacement is given by $D = \sqrt{(D'_E + D_{E0})^2 + (D'_N + D_{N0})^2}$ where D'_E and D'_N are known. The unknowns D_{E0} and D_{N0} values are determined by assuming that D_E and D_N are 0 at $t = 0$ (the time of the mainshock), and that the postseismic displacement decays following the Omori-Utsu law. Figure 5 presents two examples showing the observed displacements (D'_E and D'_N) and corrected values (D_E and D_N). We investigate the time evolutions of the postseismic displacements using the corrected data.

[29] As mentioned, we consider for the analysis only the measurements in the time period of ~3 months after the İzmit mainshock (before the Düzce earthquake). At this short time scale, the tectonic loading effect is negligible compared with the significant postseismic relaxation [*Wang et al.*, 2009]. For a simple comparison of the decay behaviors of aftershocks and aseismic deformation, we may assume that the later has the same *c* value as the former (i.e., $c_d = c_s$), and use the exponent p_d in the Omori-Utsu law as a free parameter for estimation. In this case, the two postseismic activities can be evaluated only by their decay exponent values. Since c_s is probably overestimated due to the incompleteness of the aftershock catalog immediately after the mainshock, we confine in the analysis c_d to be in the interval $(0, c_s]$.

[30] The inversion results are presented in Table 1 and Figure 6. To evaluate the confidence intervals of the estimates, accounting for both measurement uncertainty and inversion method, we additionally estimate the parameters using 100 simulated data sets with means of the real displacement values and standard deviations of 1 standard deviation of the GPS measurements. The confidence intervals of the estimates are obtained through 25% and 75% quartiles of the 100 estimates. The results in Table 1 (see also Figure 6) show that with confined c_d in the range $(0, c_s]$, the estimates of p_d and K_d based on the observed displacements are in the range of the estimates using the synthetic data with the consideration of measurement uncertainty. This indicates that the estimations are stable and reliable. The estimated p_d values with $p_d < p_s$ for all of the seven GPS stations indicate that the postseismic displacements decayed slower than the aftershock seismicity after the İzmit earthquake. For convenience, we refer to the derived results (Figure 6 and Table 1) of the Omori-type decay of the postseismic displacements as $D_{tot}(t)$. In the following sections, we investigate the contributions to the observed postseismic displacements from elastic strain changes produced by aftershocks, aftershocks/damage-induced inelastic deformation, and ductile relaxation. Additionally, we consider a simplified interseismic model for the study region to show that the tectonic motion has small effect over the studied time domain.

3.4. Different Contributions to the Whole Postseismic Displacement

3.4.1. Contribution From Tectonic Motion

[31] Here we investigate the contribution from the tectonic motion. Consistent with the employed GPS data, we first obtain the secular velocities at the seven GPS sites (Figure 7) relative to the fixed Eurasian plate according to *Wang et al.* [2009]. Secondly, we subtract the tectonic displacements from the observed postseismic measurements and fit the corrected data (denoted $D_{\bar{S}}(t)$) using the Omori-Utsu law. Thirdly, the contribution of the tectonic motion is determined by $(1 - [D_{\bar{S}}(t)/D_{tot}(t)]) \times 100\%$. The results (dashed-dotted curves in Figure 8) indicate that the tectonic motion has negligible effect on the total postseismic displacements in the first 87 days following the İzmit earthquake.

3.4.2. Contribution From Elastic Deformation Induced by Aftershocks

[32] To investigate the elastic relaxation process produced by the aftershocks, we consider the large events with $M \geq 4.0$ indicated by the black circles in Figure 2. We calculate the surface displacements produced by these aftershocks and examine their contributions to the measured postseismic

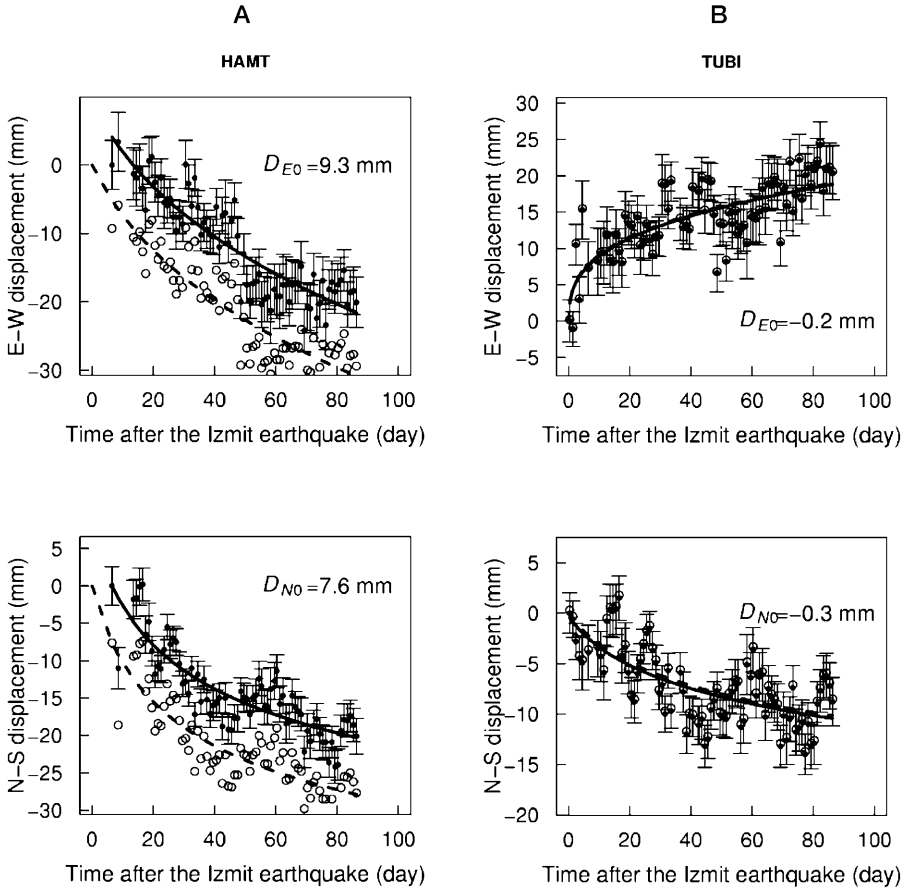

Figure 5. Two examples showing the observed (D'_E and D'_N, dots with error bars) and corrected (D_E and D_N, circles) postseismic displacements in the first 87 days following the İzmit earthquake. The corrected displacements are defined as $D_E = D'_E + D_{E0}$ and $D_N = D'_N + D_{N0}$, where D_{E0} and D_{N0} represent the postseismic displacements that occurred immediately after the mainshock and not captured by the GPS measurements. The solid and dashed curves show, respectively, the fitting results for the observed and corrected displacements based on the Omori-Utsu relation for postseismic deformation.

displacements. According to the Centroid Moment Tensor (CMT) solutions of the large aftershocks, most of the aftershocks between 29.3°E and 30.5°E have similar focal mechanism as the İzmit mainshock. We thus treat the $M \geq 4.0$ aftershocks as strike-slip events, similar to the mainshock and calculate the surface displacements at the seven GPS sites produced by these aftershocks. The calculations are done with the Okada's code, using slip values based on the empirical relation with the magnitudes [*Wells and Coppersmith*, 1994].

[33] The aftershocks used for the calculation and their displacements at the seven GPS sites are shown in Figure 9. The results indicate that the aftershock seismicity produced influential surface displacements at some GPS sites, e.g., at HAMT where the E-W displacement reaches ~7 mm in the first 87 days. After correcting for the elastic effect of the aftershocks, the postseismic displacement at HAMT site is decreased by ~20%. The contributions of the aftershocks at the other stations, $(1 - [D_{\bar{a}}(t)/D_{\mathrm{tot}}(t)]) \times 100\%$ (shown by dashed curves in Figure 8), are generally small (less than 5%),

Table 1. Estimated Parameter Values (K_d, c_d, p_d) for the Omori-Utsu Type Inelastic Deformation With c_d in $(0, c_s]$[a]

Station	K_d	c_d (day)	p_d	RMS (mm)	Distance (km)
HAMT	3.05 [2.88, 3.62]	0.81 [0.81, 0.81]	0.58 [0.55, 0.63]	2.68	5.5
MURT	4.69 [4.29, 4.92]	0.81 [0.81, 0.81]	0.60 [0.56, 0.62]	3.93	5.6
TUBI	1.89 [1.67, 2.81]	0.01 [0.01, 0.06]	0.70 [0.65, 0.80]	3.26	7.4
BEST	5.53 [5.39, 5.97]	0.81 [0.81, 0.81]	0.66 [0.65, 0.69]	4.45	12.1
UCGT	3.71 [2.46, 4.01]	0.01 [0.01, 0.01]	0.63 [0.52, 0.65]	3.70	14.0
DUMT	2.74 [2.61, 3.42]	0.01 [0.01, 0.09]	0.58 [0.57, 0.69]	3.08	17.2
KANT	1.25 [1.23, 2.27]	0.01 [0.01, 0.01]	0.75 [0.74, 0.82]	3.01	37.8

[a]'Dist' denotes the distance of the GPS sites perpendicular to latitude 40.72°N, which is the approximate location of the coseismic rupture.

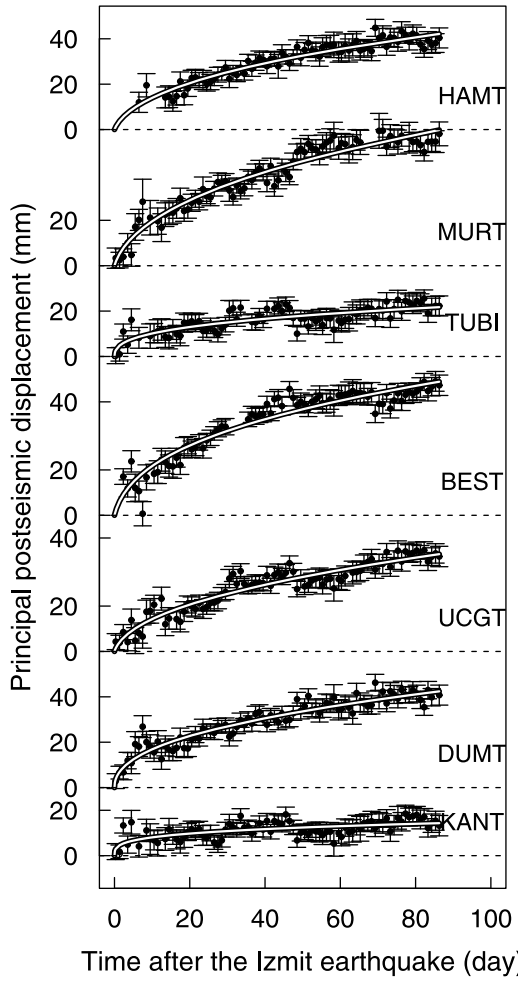

Figure 6. Principal geodetic displacements (dots with error bars) observed at seven GPS sites, and the modeling results based on the Omori-Utsu relation for postseismic deformation (white curves). The modeling assumes that the c_d parameter is confined in the interval (0, c_s] associated with the aftershock seismicity. See text for more explanations.

as has been documented [*Reilinger et al.*, 2000]. Here $D_{\bar{a}}(t)$ denotes the fit of the Omori-Utsu law to the data which are corrected from the elastic effect of the aftershocks.

3.4.3. Contribution From Damage-Related Inelastic Relaxation

[34] According to the theoretical results of section 2 and Figure 1, the damage-related inelastic deformation decays faster than the aftershock seismicity, and the decay rate for aftershock seismicity provides an upper limit for the associated inelastic relaxation rate. Therefore, the maximum damage-related aseismic deformation can be determined by setting $p_d = p_s$ and $c_d = c_s$, leading to

$$D_{\max}^{\mathrm{dam}}(t) = \frac{K_{\mathrm{d}}}{1-p_{\mathrm{s}}}\left[(c_{\mathrm{s}}+t)^{1-p_{\mathrm{s}}} - c_{\mathrm{s}}^{1-p_{\mathrm{s}}}\right]. \qquad (15)$$

Since the K_{d} parameter quantifies the magnitude of the measured postseismic displacements at different sites and is insensitive to c and p parameters in the Omori-Utsu law, we adopt the values of K_{d} in equation (15) from the numbers summarized in Table 1. The percentage of the maximum damage-related deformation among the total postseismic deformation, calculated by $D_{\max}^{\mathrm{dam}}(t)/D_{\mathrm{tot}}(t) \times 100\%$, is shown by the solid curves of Figure 8. The results indicate that the damage-related inelastic relaxation relative to the total postseismic deformation is different from site to site. However, the aftershock-related inelastic relaxation contributes generally up to 50% of the total geodetic deformation in the first 87 days.

3.4.4. Contribution From Ductile Relaxation

[35] As discussed before, the stress perturbations generated by large earthquakes are also likely to produce some stable aseismic deformation. Such deformation, represented here collectively by the ductile strain term (ε_{d} in equation (1)), may have contributions from distributed [e.g., *Wdowinski and Zilberman, 1997*; *Deng et al.*, 1998; *Wang*, 2000; *Montési*, 2004; *Perfettini and Avouac*, 2004] relaxation below the seismogenic zone. The results of the previous sections can now be used to estimate the amplitude of the combined ductile component of the observed postseismic deformation (i.e., deformation not associated with the damage-aftershocks process). Figure 10 shows the components of the postseismic

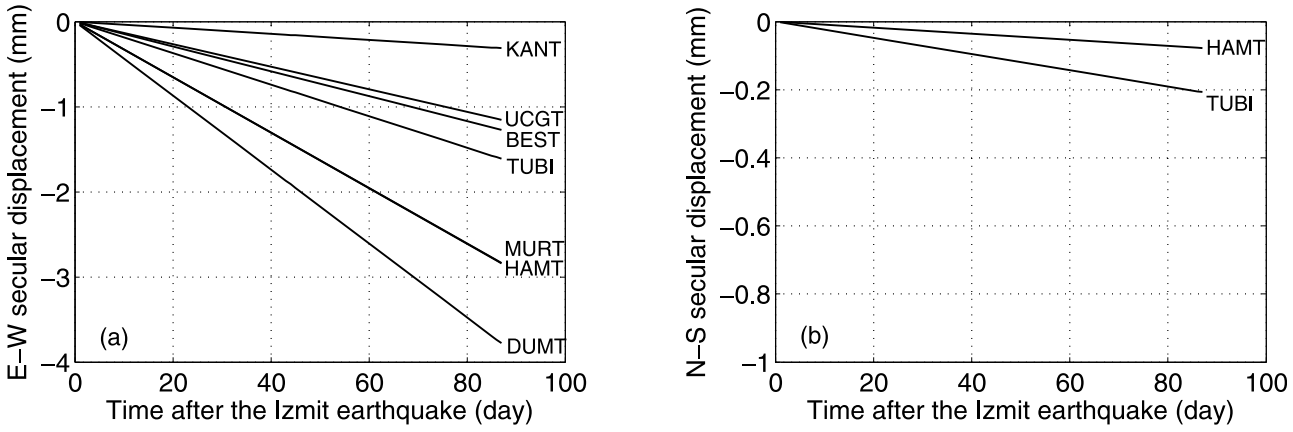

Figure 7. (a) E-W component and (b) N-S component of the tectonic motion at the seven GPS sites based on *Wang et al.* [2009]. Because the N-S displacements at the seven GPS sites are small and close to each other, only two examples are shown in Figure 7b.

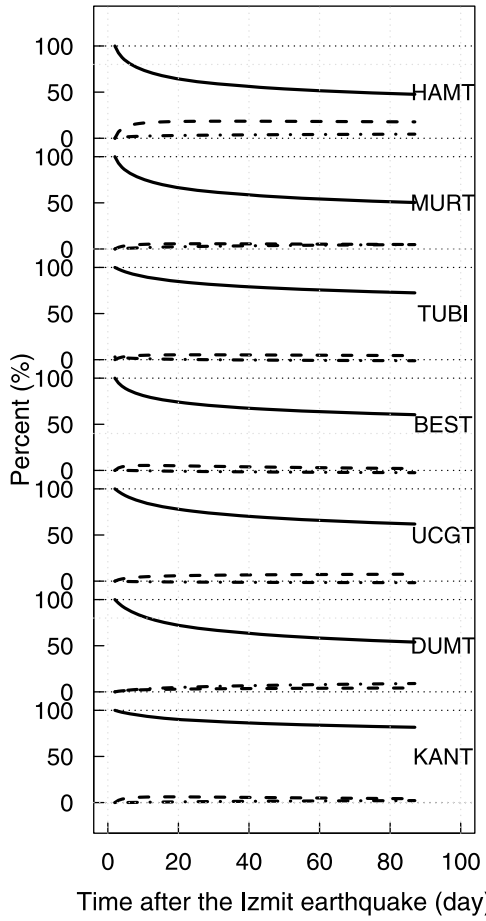

Figure 8. The contributions (percent among the total postseismic displacements) at the seven GPS sites from elastic relaxation due to aftershocks (dashed curves), tectonic motion (dashed-dotted curves), and the maximum contribution from the aftershock-induced inelastic deformation (solid curves).

measurements that may be attributed to aseismic ductile relaxation at the different sites. The results indicate that ductile relaxation was responsible for less than 50% of the postseismic deformation in the first 87 days.

4. Discussion

4.1. Frictional-Afterslip and Damage-Related Postseismic Relaxations

[36] Both aseismic deformation and aftershocks are significant phenomena following large earthquakes. Their relationship can give us clues on the roles of the two different mechanisms, frictional-afterslip and damage-related postseismic relaxation, that are assumed to occur in the local vicinity of main rupture zones.

[37] Aseismic afterslip within the framework of rate-state friction is an important candidate for explaining the postseismic deformation [*Marone et al.*, 1991]. According to rate-state friction, earthquakes nucleate in the unstable rate-weakening regime, while stable sliding occurs in the rate-strengthening regime [e.g., *Dieterich*, 1992; *Scholz*, 1998; *Ben-Zion*, 2008]. The transition between rate weakening and rate strengthening is largely thermal/depth dependent [e.g., *Blanpied et al.*, 1991]. For the continental crust, the transition occurs approximately at 15–20 km depth, corresponding to temperature of ~300°C. The region near the surface (less than 2–3 km depth) is also likely governed by rate strengthening because of poorly consolidated material [*Marone et al.*, 1991]. In addition, rate strengthening may be produced by specific minerals and rock types such as serpentinite [e.g., *Sato et al.*, 1984] or other unusual local properties. However, a given location on the fault is either rate weakening (in which case brittle instabilities and hypocenters may be generated) or rate strengthening (in which case only stable slip occurs). Thus, in the framework of rate-state friction, the spatial distributions of aftershocks seismicity and aseismic afterslip should be anticorrelated. High-resolution observations, such as those available along the Parkfield section of the San Andreas fault, show clearly that the seismic and aseismic regions along fault are disjointed [e.g., *Thurber et al.*, 2006].

[38] In contrast to the frictional-afterslip framework, associated with highly localized fault (or a small set of fault

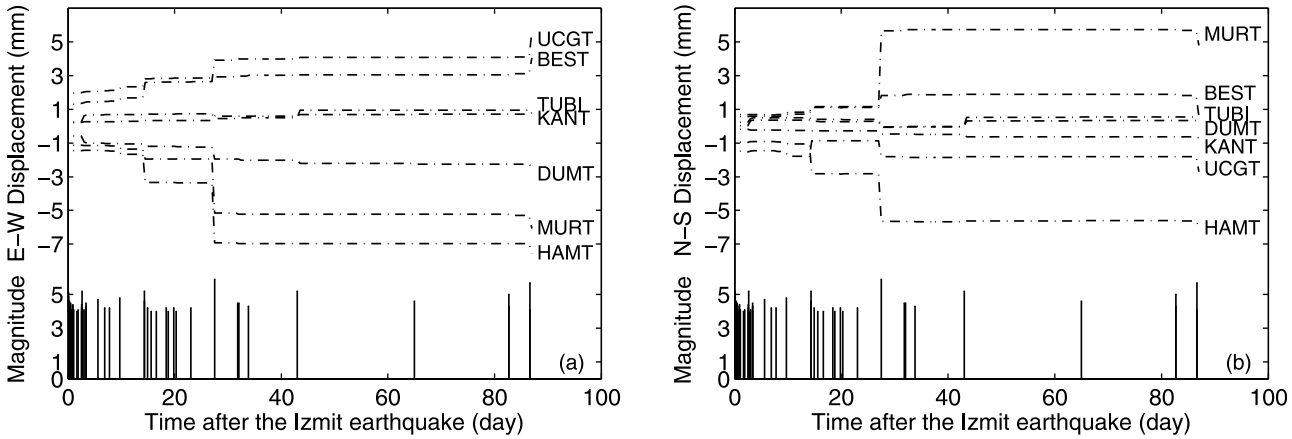

Figure 9. *M-t* plot ($M \geq 4.0$) and the calculated (a) E-W and (b) N-S displacements associated with elastic relaxation produced by the aftershocks at the seven GPS sites.

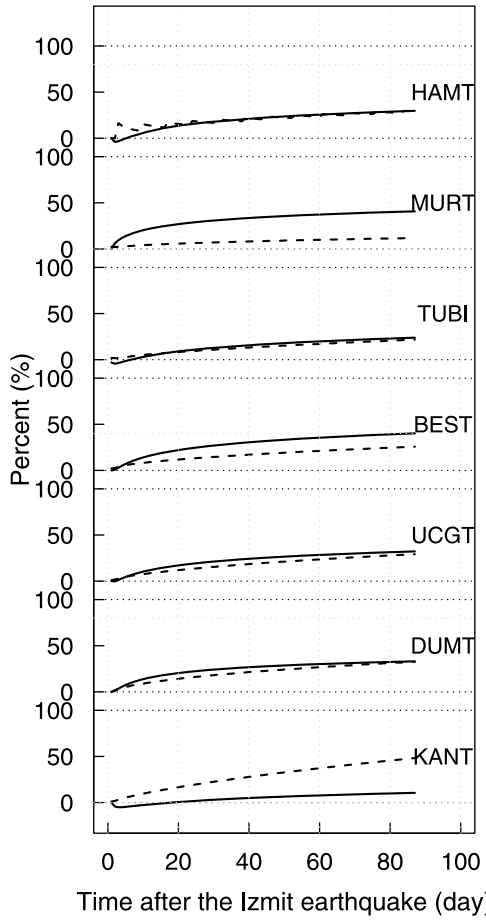

Figure 10. The percentage of the residual displacement (excluding aftershocks-induced elastic/inelastic deformation and tectonic motion) among the observed postseismic displacements (solid curves). The dashed curves show the percentage of the estimated distributed ductile relaxation in the lower crust and upper mantle based on the rheological model of *Wang et al.* [2009].

surfaces) with fixed rate-strengthening rheological parameters, the damage rheology framework is associated with volumetric cracking that (among other things) reduces the effective viscosity of the brittlely deforming regions. The reduced effective viscosity during the occurrence of high rate seismicity (aftershocks) leads to relaxation that produces geodetic deformation. The employed damage rheology was shown to be consistent with detailed laboratory results of fracture and friction experiments [e.g., *Hamiel et al.*, 2004; *Lyakhovsky et al.*, 2009; *Hamiel et al.*, 2009] and various observed spatio-temporal patterns of earthquakes and faults [e.g., *Ben-Zion and Lyakhovsky*, 2002; *Finzi et al.*, 2009]. In particular, theoretical studies have shown that the damage model can describe the main phenomenological features of aftershock sequences [*Ben-Zion and Lyakhovsky*, 2006] as well as rate-state friction [*Lyakhovsky et al.*, 2005]. The damage process is associated fundamentally with volumes rather than surfaces, and significant damage-related transient postseismic relaxation is expected to occur in the volume around the main rupture zone where aftershocks densely occur.

[39] It is difficult to distinguish the damage-related relaxation and frictional-afterslip based only on slip inversions of geodetic measurements, as is the case for a distinction between viscoelastic relaxation in the ductile layer from deep afterslip [*Thatcher*, 1983; *Savage*, 1990]. However, the degree of spatial correlation (or anticorrelation) between fault regions with high aftershocks activity and high postseismic slip provides a way for distinguishing between damage-related relaxation and frictional afterslip. As mentioned in section 3.1, *Çakir et al.* [2003] found strong correlation between aftershocks activity and postseismic slip following the İzmit mainshock. This implies that the damage-related relaxation process is significant, at least around sections of the İzmit rupture zone where there is large overlap between dense aftershocks and inferred postseismic deformation.

4.2. Postseismic Relaxation in the Deep Ductile Zone Following the İzmit Earthquake

[40] Starting from basic relations between local brittle failures and gradual inelastic strain in the framework of the viscoelastic damage rheology model [*Ben-Zion and Lyakhovsky*, 2006], we obtain a relation between the decay rates of aftershocks and the related postseismic deformation. This enables us to quantify effectively the aftershocks-induced postseismic relaxation and attribute the remainder (non-aftershocks-induced) portion of the observed displacements to aseismic processes represented collectively by the ductile strain of equation (1).

[41] *Wang et al.* [2009] tested several rheological models based on the postseismic displacements observed over 6 years following the İzmit earthquake. They found that a rheological model consisting of elastic upper crust, inelastic lower crust described by Maxwell rheology overlaying a Maxwell upper mantle substrate, with effective viscosities of 2×10^{19} Pa s and 7×10^{19} Pa s for the lower crust and upper mantle, best fits the velocity measurements in 4–6 years after the mainshock. Similar effective viscosities were derived by other studies [e.g., *Hearn et al.*, 2009]. Based on the GPS measurements in 2.5 years following the İzmit event, *Hearn et al.* [2009] found that the viscoelastic relaxation in the lower crust and upper mantle with viscosities of 2×10^{19} to 5×10^{19} Pa s provide better fit for the postseismic displacements after some months following the İzmit event. Therefore, an effective viscosity of $\sim 2–5 \times 10^{19}$ Pa s is likely an approximation to the rheology at the time scale of years following the İzmit earthquake.

[42] *Wang et al.* [2009] also considered transient rheology to model the postseismic displacements following the İzmit earthquake. Using both short-term (during 1 year after the İzmit event) postseismic displacements in the far-field (>30 km from the fault) and long-term (4–6 years after the mainshock) displacements, *Wang et al.* [2009] developed a three-layer model (E-SLS-M, elastic upper crust, inelastic lower crust described by Standard Linear Solid rheology, overlaying a Maxwell upper mantle). They found that the lower crust has effective viscosity of 2×10^{18} Pa s and relaxation strength of 2/3, and the upper mantle has effective viscosity of 7×10^{19} Pa s. *Wang et al.* [2009] showed that the stable slip inverted from the postseismic data after correcting for the relaxation component predicted from the E-SLS-M model concentrates mainly in the elastic layer.

Thus, the E-SLS-M model describes the relaxation in the deep ductile zone during the postseismic interval. On the other hand, *Hetland* [2006] constructed a two-layer model (elastic crust overlaying inelastic mantle described by Burgers' rheology), which provides an effective viscosity of 0.4×10^{19} to 1×10^{19} Pa s for transient deformation. The estimated viscosity of the two-layer model [*Hetland*, 2006] corresponds the average value of the estimates in the three-layer model [*Wang et al.*, 2009].

[43] Given the above ranges of results, we adopt the E-SLS-M model [*Wang et al.*, 2009] to quantify the relaxation component in the deep ductile zone. We calculate the contribution of the deep relaxation to the observed postseismic deformation at the seven GPS sites. The results shown by the dashed curves in Figure 10 indicate that the residual postseismic displacements, left after subtracting the contributions from the aftershock-induced elastic/inelastic deformation and the tectonic motion, can be attributed at most GPS sites to deep ductile relaxation described by the E-SLS-M model. The observed deformation cannot be completely explained by a combination of aftershock-induced and ductile effects, which might indicate some local rheological heterogeneity, only at sites MURT, BEST and KANT.

[44] In the eastern section of sites MURT and BEST, tomography studies show comparatively higher *P* wave velocities and higher *Q* values suggesting colder and more brittle material [*Nakamura et al.*, 2002; *Koulakov et al.*, 2010]. Based on the results of *Ben-Zion and Lyakhovsky* [2006], cold brittle material is expected to produce long Omori-type aftershock sequence with relatively low *p* value and high event productivity. Therefore, when we applied the constraint $p_d = p_s$ (in section 3.3.3 a homogenous p_s value has been determined for the entire study region) for the geodetic deformation, we likely underestimated the aftershocks-induced aseismic deformation in this area. On the other hand, the deformation summation due to aftershocks-induced inelastic relaxation and distributed ductile relaxation overestimates the postseismic displacement at site KANT. We note that KANT is far from the fault damage zone and the surrounding aftershock seismicity is rather low. Thus, our simple procedure overestimated the damage-related deformation at this site (cf. Figure 9) and produced modeled postseismic displacement that is higher than the observed displacement (cf. Figure 10).

5. Conclusion

[45] We developed quantitative results associated with damage-related postseismic deformation, which can explain the observed postseismic relaxation in the seismogenic zone, particularly in areas with high aftershock activity. Assuming that the Omori-Utsu law describes the aftershocks rate, we show that the damage-related inelastic deformation follows a generalized Omori-Utsu type decay with the standard Omori-Utsu law as a limit case (section 2). The obtained theoretical results can be used to separate (to first order) between brittle and ductile contributions to postseismic deformation, which are dominant in the shallow seismogenic zone and the deeper ductile region, respectively.

[46] To test and illustrate the obtained theoretical expressions, we analyzed the observed GPS displacements at the sites around the rupture zone of the 1999 İzmit earthquake. The results (section 3) can be summarized as follows. (1) The entire postseismic displacement measured on the surface decayed slower than the aftershock seismicity in the first 87 days after the İzmit earthquake. (2) The aftershocks/damage-related relaxation can maximally account for up to 50% of the total deformation. (3) The remainder postseismic displacement can be largely explained by the relaxation at the deeper section based on the E-SLS-M rheological model reported by *Wang et al.* [2009]. (4) The contribution from aftershocks-induced elastic relaxation is generally less than 10% of the observed postseismic displacements, but it can be influential at some individual sites. (5) The tectonic motion is negligible in the examined time interval.

[47] It is important to examine in future studies whether the theoretical results and partitioning of observed surface geodetic deformation obtained in this work apply in a similar way to other cases of postseismic deformation.

[48] **Acknowledgments.** We are grateful to Semih Ergintav for providing us the GPS data, to Bogdan Enescu for discussions at the early stage of this work, and to Eric Hetland and two anonymous reviewers for constructive comments. L. Wang thanks the DAAD (Deutscher Akademischer Austausch Dienst) for providing financial support for her Ph.D. studies.

References

Aktar, M., S. Özalaybey, M. Ergin, H. Karabulut, M.-P. Bouin, C. Tapırdamaz, F. Biçmen, A. Yörük, and M. Bouchon (2004), Spatial variation of aftershock activity across the rupture zone of the 17 August 1999 Izmit earthquake, Turkey, *Tectonophysics*, *391*(1–4), 325–334, doi:10.1016/j.tecto.2004.07.020.

Barbot, S., Y. Hamiel, and Y. Fialko (2008), Space geodetic investigation of the coseismic and postseismic deformation due to the 2003 M_w7.2 Altai earthquake: Implications for the local lithospheric rheology, *J. Geophys. Res.*, *113*, B03403, doi:10.1029/2007JB005063.

Ben-Zion, Y. (2008), Collective behavior of earthquakes and faults: Continuum-discrete transitions, progressive evolutionary changes, and different dynamic regimes, *Rev. Geophys.*, *46*, RG4006, doi:10.1029/2008RG000260.

Ben-Zion, Y., and V. Lyakhovsky (2002), Accelerated seismic release and related aspects of seismicity patterns on earthquake faults, *Pure Appl. Geophys.*, *159*(10), 2385–2412, doi:10.1007/s00024-002-8740-9.

Ben-Zion, Y., and V. Lyakhovsky (2006), Analysis of aftershocks in a lithospheric model with seismogenic zone governed by damage rheology, *Geophys. J. Int.*, *165*(1), 197–210, doi:10.1111/j.1365-246X.2006.02878.x.

Ben-Zion, Y., J. R. Rice, and R. Dmowska (1993), Interaction of the San Andreas fault creeping segment with adjacent great rupture zones, and earthquake recurrence at Parkfield, *J. Geophys. Res.*, *98*, 2,135–2,144.

Ben-Zion, Y., Z. Peng, D. Okaya, L. Seeber, J. G. Armbruster, N. Ozer, A. J. Michael, S. Baris, and M. Aktar (2003), A shallow fault-zone structure illuminated by trapped waves in the Karadere-Duzce branch of the North Anatolian Fault, western Turkey, *Geophys. J. Int.*, *152*(3), 699–717, doi:10.1046/j.1365-246X.2003.01870.x.

Blanpied, M. L., D. A. Lockner, and J. D. Byerlee (1991), Fault stability inferred from granite sliding experiments at hydrothermal conditions, *Geophys. Res. Lett.*, *18*, 609–612.

Bohnhoff, M., H. Grosser, and G. Dresen (2006), Strain partitioning and stress rotation at the North Anatolian fault zone from aftershock focal mechanisms of the 1999 Izmit M_w = 7.4 earthquake, *Geophys. J. Int.*, *166*(1), 373–385, doi:10.1111/j.1365-246X.2006.03027.x.

Bürgmann, R., P. Segall, M. Lisowski, and J. Svarc (1997), Postseismic strain following the 1989 Loma Prieta earthquake from GPS and leveling measurements, *J. Geophys. Res.*, *102*, 4,933–4,955.

Bürgmann, R., S. Ergintav, P. Segall, E. H. Hearn, S. McClusky, R. E. Reilinger, H. Woith, and J. Zschau (2002), Time-dependent distributed afterslip on and deep below the İzmit earthquake rupture, *Bull. Seismol. Soc. Am.*, *92*(1), 126–137.

Çakir, Z., J.-B. de Chabalier, R. Armijo, B. Meyer, A. Barka, and G. Peltzer (2003), Coseismic and early post-seismic slip associated with the 1999 Izmit earthquake (Turkey), from SAR interferometry and tectonic field observations, *Geophys. J. Int.*, *155*(1), 93–110.

Chester, F. M. (1995), A rheologic model for wet crust applied to strike-slip faults, *J. Geophys. Res.*, *100*, 13,033–13,044.

Chester, F. M., J. P. Evans, and R. L. Biegel (1993), Internal structure and weakening mechanisms of the San Andreas fault, *J. Geophys. Res.*, *98*, 771–786.

Daniel, G., D. Marsan, and M. Bouchon (2006), Perturbation of the Izmit earthquake aftershock decaying activity following the 1999 M_w 7.2 Düzce, Turkey, earthquake, *J. Geophys. Res.*, *111*, B05310, doi:10.1029/2005JB003978.

Deng, J., M. Gurnis, H. Kanamori, and E. Hauksson (1998), Viscoelastic flow in the lower crust after the 1992 Landers, California, earthquake, *Science*, *282*(5394), 1,689–1,692.

Dieterich, J. H. (1992), Earthquake nucleation on faults with rate- and state-dependent strength, *Tectonophysics*, *211*, 115–134.

Enescu, B., J. Mori, and M. Miyazawa (2007), Quantifying early aftershock activity of the 2004 mid-Niigata Prefecture earthquake (M_w6.6), *J. Geophys. Res.*, *112*, B04310, doi:10.1029/2006JB004629.

Ergintav, S., R. Bürgmann, S. McClusky, R. Çakmak, R. E. Reilinger, O. Lenk, A. Barka, and H. Özener (2002), Postseismic deformation near the İzmit earthquake (17 August 1999, *M* 7.5) rupture zone, *Bull. Seismol. Soc. Am.*, *92*(1), 194–207.

Ergintav, S., S. McClusky, E. Hearn, R. Reilinger, R. Cakmak, T. Herring, H. Ozener, O. Lenk, and E. Tari (2009), Seven years of postseismic deformation following the 1999, M = 7.4 and M = 7.2, Izmit-Düzce, Turkey earthquake sequence, *J. Geophys. Res.*, *114*, B07403, doi:10.1029/2008JB006021.

Fialko, Y. (2004), Evidence of fluid-filled upper crust from observations of postseismic deformation due to the 1992 M_w7.3 Landers earthquake, *J. Geophys. Res.*, *109*, B08401, doi:10.1029/2004JB002985.

Fialko, Y., D. Sandwell, D. Agnew, M. Simons, P. Shearer, and B. Minster (2002), Deformation on nearby faults induced by the 1999 Hector Mine earthquake, *Science*, *297*(5588), 1,858–1,862, doi:10.1126/science.1074671.

Finzi, Y., E. H. Hearn, Y. Ben-Zion, and V. Lyakhovsky (2009), Structural properties and deformation patterns of evolving strike-slip faults: Numerical simulations incorporating damage rheology, *Pure Appl. Geophys.*, *166*, 1,537–1,573, doi:10.1007/s00024-009-0522-1.

Freed, A. W., and R. Bürgmann (2004), Evidence of power-law flow in the Mojave desert mantle, *Nature*, *430*(6999), 548–551, doi:10.1038/nature02784.

Hamiel, Y., Y. Liu, V. Lyakhovsky, Y. Ben-Zion, and D. Lockner (2004), A viscoelastic damage model with applications to stable and unstable fracturing, *Geophys. J. Int.*, *159*(3), 1155–1165, doi:10.1111/j.1365-246X.2004.02452.x.

Hamiel, Y., V. Lyakhovsky, S. Stanchits, G. Dresen, and Y. Ben-Zion (2009), Brittle deformation and damage-induced seismic wave anisotropy in rocks, *Geophys. J. Int.*, *178*, 901–909, doi:10.1111/j.1365-246X.2009.04200.x.

Hearn, E. H., R. Bürgmann, and R. E. Reilinger (2002), Dynamics of İzmit earthquake postseismic deformation and loading of the Düzce earthquake hypocenter, *Bull. Seismol. Soc. Am.*, *92*(1), 172–193.

Hearn, E. H., S. McClusky, R. Reilinger, and S. Ergintav (2006), Earthquake-cycle models as tie-breakers: Assessing candidate rheologies for ongoing Izmit earthquake postseismic deformation, *Eos Trans. AGU*, *87*(52), Fall Meet. Suppl., Abstract G32A-03.

Hearn, E. H., S. McClusky, S. Ergintav, and R. E. Reilinger (2009), Izmit earthquake postseismic deformation and dynamics of the North Anatolian Fault Zone, *J. Geophys. Res.*, *114*, B08405, doi:10.1029/2008JB006026.

Hetland, E. (2006), Models of interseismic deformation with an analytic framework for the inclusion of general linear viscoelastic rheologies, Ph.D. dissertation, Mass. Inst. Technol., Cambridge.

Hetland, E. A., and B. H. Hager (2006), The effects of rheological layering on post-seismic deformation, *Geophys. J. Int.*, *166*(1), 277–292, doi:10.1111/j.1365-246X.2006.02974.x.

Hsu, Y.-J., N. Bechor, P. Segall, S.-B. Yu, L.-C. Kuo, and K.-F. Ma (2002), Rapid afterslip following the 1999 Chi-Chi, Taiwan earthquake, *Geophys. Res. Lett.*, *29*(16), 1754, doi:10.1029/2002GL014967.

Hsu, Y.-J., M. Simons, J.-P. Avouac, J. Galetzka, K. Sieh, M. Chlieh, D. Natawidjaja, L. Prawirodirdjo, and Y. Bock (2006), Frictional afterslip following the 2005 Nias-Simeulue earthquake, Sumatra, *Science*, *312*(5782), 1921–1926, doi:10.1126/science.1126960.

Hsu, Y.-J., S.-B. Yu, and H.-Y. Chen (2009), Coseismic and postseismic deformation associated with the 2003 Chengkung, Taiwan, earthquake, *Geophys. J. Int.*, *176*(2), 420–430, doi:10.1111/j.1365-246X.2008.04009.x.

Jónsson, S., P. Segall, R. Pedersen, and G. Björnsson (2003), Post-earthquake ground movements correlated to pore-pressure transients, *Nature*, *424*(6945), 179–183, doi:10.1038/nature01776.

Koulakov, I., D. Bindi, S. Parolai, H. Grosser, and C. Milkereit (2010), Distribution of seismic parameters (V_P, V_S, V_P/V_S and frequency-dependent Q_S) in the crust beneath the North Anatolian fault (Turkey) from local earthquake tomographic inversion, *Bull. Seismol. Soc. Am.*, *100*(1), 207–224, doi:10.1785/0120090105.

Li, V. C., and J. R. Rice (1987), Crustal deformation in great California earthquakes, *J. Geophys. Res.*, *92*, 11,533–11,551.

Lolli, B., and P. Gasperini (2006), Comparing different models of aftershock rate decay: The role of catalog incompleteness in the first times after main shock, *Tectonophysics*, *423*(1–4), 43–59, doi:10.1016/j.tecto.2006.03.025.

Lorenzo-Martín, F., F. Roth, and R. Wang (2006), Elastic and inelastic triggering of earthquakes in the North Anatolian Fault zone, *Tectonophysics*, *424*(3–4), 271–289, doi:10.1016/j.tecto.2006.03.046.

Lyakhovsky, V., Y. Ben-Zion, and A. Agnon (1997), Distributed damage, faulting, and friction, *J. Geophys. Res.*, *102*(B12), 27,635–27,649.

Lyakhovsky, V., Y. Ben-Zion, and A. Agnon (2001), Earthquake cycle, fault zones, and seismicity patterns in a rheologically layered lithosphere, *J. Geophys. Res.*, *106*(B3), 4,103–4,120.

Lyakhovsky, V., Y. Ben-Zion, and A. Agnon (2005), A viscoelastic damage rheology and rate- and state-dependent friction unstable fracturing, *Geophys. J. Int.*, *161*(1), 179–190, doi:10.1111/j.1365-246X.2005.02583.x.

Lyakhovsky, V., Y. Hamiel, J. P. Ampuero, and Y. Ben-Zion (2009), Nonlinear damage rheology and wave resonance in rocks, *Geophys. J. Int*, *178*, 910–920, doi:10.1111/j.1365-246X.2009.04205.x.

Mahsas, A., K. Lammali, K. Yelles, E. Calais, A. M. Freed, and P. Briole (2008), Shallow afterslip following the 2003 May 21, *M*w = 6.9 Boumerdes earthquake, Algeria, *Geophys. J. Int*, *172*, 155–166, doi:10.1111/j.1365-246X.2007.03594.x.

Marone, C., and C. H. Scholz (1988), The depth of seismic faulting and the upper transition from stable to unstable slip regimes, *Geophys. Res. Lett.*, *15*(6), 621–624.

Marone, S. G., C. H. Scholz, and R. Bilham (1991), On the mechanics of earthquake afterslip, *J. Geophys. Res.*, *96*(B5), 8,441–8,452.

Masterlark, T., and H. F. Wang (2002), Transient stress-coupling between the 1992 Landers and 1999 Hector Mine earthquakes, *Bull. Seismol. Soc. Am.*, *92*, 1,470–1,486.

Miyazaki, S., P. Segall, J. Fukuda, and T. Kato (2004), Space time distribution of afterslip following the 2003 Tokachi-oki earthquake: Implications for variations in fault zone frictional properties, *Geophys. Res. Lett.*, *31*, L06623, doi:10.1029/2003GL019410.

Montési, L. G. J. (2004), Controls of shear zone rheology and tectonic loading on postseismic creep, *J. Geophys. Res.*, *109*, B10404, doi:10.1029/2003JB002925.

Nakamura, A., et al. (2002), *P*-wave velocity structure of the crust and its relationship to the occurrence of the 1999 İzmit, Turkey, earthquake and aftershocks, *Bull. Seismol. Soc. Am.*, *92*(1), 330–338.

Nur, A., and J. D. Byerlee (1971), An effective stress law for elastic deformation of rocks with fluids, *J. Geophys. Res.*, *76*, 66,414–66,419.

Owen, S., G. Anderson, D. C. Agnew, H. Johnson, K. Hurst, R. Reilinger, Z.-K. Shen, J. Svarc, and T. Baker (2002), Early postseismic deformation from the 16 October 1999 M_w 7.1 Hector Mine, California, earthquake as measured by survey-mode GPS, *Bull. Seismol. Soc. Am.*, *92*(4), 1,423–1,432.

Peltzer, G., P. Rosen, F. Rogez, and K. Hudnut (1998), Poroelastic rebound along the Landers 1992 earthquake surface rupture, *J. Geophys. Res.*, *103*(B12), 30,131–30,146.

Peng, Z., and Y. Ben-Zion (2006), Temporal changes of shallow seismic velocity around the Karadere-Düzce Branch of the north Anatolian fault and strong ground motion, *Pure Appl. Geophys.*, *163*, 567–600, doi:10.1007/s00024-005-0034-6.

Peng, Z., J. E. Vidale, and H. Houston (2006), Anomalous early aftershock decay rate of the 2004 Mw6.0 Parkfield, California, earthquake, *Geophys. Res. Lett.*, *33*, L17307, doi:10.1029/2006GL026744.

Perfettini, H., and J.-P. Avouac (2004), Postseismic relaxation driven by brittle creep: A possible mechanism to reconcile geodetic measurements and the decay rate of aftershocks, application to the Chi-Chi earthquake, Taiwan, *J. Geophys. Res.*, *109*, B02304, doi:10.1029/2003JB002488.

Perfettini, H., J.-P. Avouac, and J.-C. Ruegg (2005), Geodetic displacements and aftershocks following the 2001 M_w = 8.4 Peru earthquake: Implications for the mechanics of the earthquake cycle along subduction zones, *J. Geophys. Res.*, *110*, B09404, doi:10.1029/2004JB003522.

Pollitz, F. F., R. Bürgmann, and P. Segall (1998), Joint estimation of afterslip rate and postseismic relaxation following the 1989 Loma Prieta earthquake, *J. Geophys. Res.*, *103*, 26,975–26,992.

Pollitz, F. F., G. Peltzer, and R. Bürgmann (2000), Mobility of continental mantle: Evidence from postseismic geodetic observations following the 1992 Landers earthquake, *J. Geophys. Res.*, *105*(B4), 8,035–8,054, doi:10.1029/1999JB900380.

Reilinger, R. E., et al. (2000), Coseismic and postseismic fault slip for the 17 August 1999, $M = 7.5$, Izmit, Turkey earthquake, *Science*, *289*(5484), 1519–1523, doi:10.1126/science.289.5484.1519.

Rice, J. R., and M. P. Cleary (1976), Some basic stress diffusion solutions for fluid-saturated elastic porous media with compressible constituents, *Rev. Geophys. Space Phys.*, *14*, 227–241.

Rubinstein, J. L., N. Uchida, and G. C. Beroza (2007), Seismic velocity reductions caused by the 2003 Tokachi-Oki earthquake, *J. Geophys. Res.*, *112*, B05315, doi:10.1029/2006JB004440.

Ryder, I., B. Parsons, T. J. Wright, and G. J. Funning (2007), Post-seismic motion following the 1997 Manyi (Tibet) earthquake: InSAR observations and modelling, *Geoph. J. Int.*, *169*(3), 1,009–1,027, doi:10.1111/j.1365-246X.2006.03312.x.

Sato, M., A. J. Sutton, and K. A. McGee (1984), Anomalous hydrogen emissions from the San Andreas fault observed at the Cienega Winery, central California, *Pure Appl. Geophys.*, *122*(2–4), 376–391, doi:10.1007/BF00874606.

Savage, J. C. (1990), Equivalent strike-slip earthquake cycles in half-space and lithosphere-asthenosphere earth models, *J. Geophys. Res.*, *95*, 4,873–4,879.

Savage, J. C., and J. L. Svarc (1997), Postseismic deformation associated with the 1992 Mw = 7.3 Landers earthquake, southern California, *J. Geophys. Res.*, *102*(B4), 7565–7577, doi:10.1029/97JB00210.

Savage, J. C., and J. L. Svarc (2009), Postseismic relaxation following the 1992 7.3 Landers and 1999 7.1 Hector Mine earthquakes, southern California, *J. Geophys. Res.*, *114*, B01401, doi:10.1029/2008JB005938.

Savage, J. C., J. L. Svarc, and S.-B. Yu (2007), Postseismic relaxation and aftershocks, *J. Geophys. Res.*, *112*, B06406, doi:10.1029/2006JB004584.

Sawazaki, K., H. Sato, H. Nakahara, and T. Nishimura (2006), Temporal change in site response caused by earthquake strong motion as revealed from coda spectral ratio measurement, *Geophys. Res. Lett.*, *33*, L21303, doi:10.1029/2006GL027938.

Scholz, C. H. (1998), Earthquakes and friction laws, *Nature*, *391*, 37–42.

Shen, Z.-K., D. D. Jackson, Y. Feng, M. Cline, M. Kim, P. Fang, and Y. Bock (1994), Postseismic deformation following the Landers earthquake, California, 28 June 1992, *Bull. Seism. Soc. Am.*, *84*, 780–791.

Thatcher, W. (1983), Nonlinear strain buildup and the earthquake cycle on the San Andreas fault, *J. Geophys. Res.*, *88*, 5893-5902.

Thurber, C. H., H. Zhang, F. Waldhauser, J. Hardebeck, A. Michael, and D. Eberhart-Phillips (2006), Three-dimensional compressional wavespeed model, earthquake relocations, and focal mechanisms for the Parkfield, California, region, *Bull. Seismol. Soc. Am.*, *96*(4B), S38–S49, doi:10.1785/0120050825.

Toksöz, M. N., A. F. Shakal, and A. J. Michael (1979), Space-time migration of earthquakes along the North Anatolian fault zone and seismic gaps, *Pure Appl. Geoph.*, *117*, 1258–1270.

Utsu, T., Y. Ogata, and R. S. Matsu'ura (1995), The centenary of the Omori formula for a decay law of aftershock activity, *J. Phys. Earth*, *43*, 1–33.

Wang, H. F. (2000), *Theory of Linear Poroelasticity with Applications to Geomechanics and Hydrogeology*, 276 pp., Princeton Univ. Press, Princeton.

Wang, L., R. Wang, F. Roth, B. Enescu, S. Hainzl, and S. Ergintav (2009), Afterslip and viscoelastic relaxation following the 1999 $M7.4$ Izmit earthquake from GPS measurements, *Geophys. J. Int.*, *178*, 1220–1237, doi:10.1111/j.1365-246X.2009.04228.x.

Wdowinski, S., and E. Zilberman (1997), Systematic analyses of the large-scale topography and across the Dead Sea Rift, *Tectonics*, *16*, 409–424.

Wells, D. W., and K. J. Coppersmith (1994), New empirical relationships among magnitude, rupture length, rupture width, rupture area, and surface displacement, *Bull. Seismol. Soc. Am.*, *84*(4), 974–1002.

Wright, T., E. Fielding, and B. Parsons (2001), Triggered slip: observations of the 17 August 1999 Izmit (Turkey) earthquake using radar interferometry, *Geophys. Res. Lett.*, *28*(6), 1079–1082.

Wu, C., Z. Peng, and Y. Ben-Zion (2009), Non-linearity and temporal changes of fault zone site response associated with strong ground motion, *Geophys. J. Int*, *176*, 265–278, doi:10.1111/j.1365-246X.2008.04005.x.

Yu, S.-B., Y.-J. Hsu, L.-C. Kuo, H.-Y. Chen, and C.-C. Liu (2003), GPS measurement of postseismic deformation following the 1999 Chi-Chi, Taiwan, earthquake, *J. Geophys. Res.*, *108*(B11), 2520, doi:10.1029/2003JB002396.

Y. Ben-Zion, Department of Earth Sciences, University of Southern California, Los Angeles, CA, 90089-0740, USA.

S. Hainzl, Deutsches GeoForschungsZentrum, Telegrafenberg, Potsdam, Germany, D-14473.

M. Sinan Özeren, Istanbul Technical University, Istanbul, 34398, Turkey.

L. Wang, Deutsches GeoForschungsZentrum, Telegrafenberg, Section 2.1, Potsdam, D-14473, Germany. (wanglf@gfz-potsdam.de)